RSC Advances

PAPER

View Article Online
View Journal | View Issue

Cite this: *RSC Adv.*, 2014, **4**, 47670

Electrochromic response of pulsed laser deposition prepared WO_3–TiO_2 composite film

Liying Wang, Long Yuan, Xiaofeng Wu, Jie Wu, Changmin Hou* and Shouhua Feng

Received 15th July 2014
Accepted 11th September 2014

DOI: 10.1039/c4ra07138g

www.rsc.org/advances

Electrochromic films of WO_3 with varying content of TiO_2, as a composite, were prepared *via* pulsed laser deposition method. The composite films exhibited cathodic electrochromism, which changed the original colorless appearance to a deep blue color. The films were examined for their structure, morphology, ultraviolet to visible photon absorption and chromic changes in electric fields. Pure WO_3 film showed stronger absorption at 600–800 nm wavelength of light than the composite films, which corresponds to blue color. The most intensive absorption wavelength of light could be modulated with TiO_2 inclusion, leading to a respective color change from dark blue to gem blue of the as-deposited WO_3–TiO_2–ITO glass. This work may serve as a basis for electrochromic windows and display device applications.

1. Introduction

Chromic materials and electrochromics

Electrochromic devices have been increasingly applied in large-area display devices, switchable mirrors and smart windows.[1,2] The most potential application of electrochromics lies in windows to regulate heat and light flow.[3] Electrochromic films can be deposited as thin layers (0.1–0.4 mm) onto a transparent substrate.[4] The microstructure of electrochromic films plays an important role in their kinetics, durability, coloring efficiency and storage capacity.[5] A number of materials, such as transition metal oxides, mixed valence materials,[6] organic molecules[7] and conjugated polymers,[8] and hybrid materials,[9] have been reported to display such electrochromic properties. The ability to reversibly change the absorption of different positions of photo waves in electrochromic materials has attracted interest for applications in technologies such as smart windows[6] and electronic papers.[10,11] Traditionally, metal oxide electrochromic materials are transition metal oxide films such as WO_3,[12,13] TiO_2,[14,15] Nb_2O_5,[16] MoO_3,[17] and $Ni(OH)_2$.[18] Blue color glass films have been widely applied in room light modulation. Hence, we attempted to modulate the transmittance of light by WO_3 films with the aid of TiO_2 doping.

WO_3 and TiO_2-doped WO_3 films

The first sol–gel synthesis of electrochromic WO_3 was reported 30 years ago.[19] The lifetime of coloration-bleaching electrochromic cycling depends on the crystallographic structure (amorphous or crystalline phases) of $WO_3 \cdot nH_2O$ films prepared at discrete experimental conditions (*e.g.*, pH, concentration and temperature).[20] Dip-coating and calcination method can produce WO_3 films with good electrochromic properties, where hydrogen peroxide is added to a tungsten acid solution.[21] The success of TiO_2-doped WO_3 films was first reported on an ITO-coated glass substrate by the spin-coating method. The poor electrochromic properties of the 350 °C annealed films could be significantly improved by exposure to air for 1 week, which can be attributed to the accelerating role of adsorbed water during lithium insertion into the WO_3–TiO_2 films.[22] Aqueous solutions of sodium tungstate (Na_2WO_4) and dimethyl sulfate ($(CH_3)_2SO_4$) were used to deposit WO_3 films on fluorine-doped SnO_2 in sulfuric acid with a high film durability of around 7000 cycles by cyclic voltammetry test.[23] By incorporating polystyrene microspheres into the precursor of the sols of TiO_2–WO_3 composite, porous films could be prepared, which improves the electrochromic properties compared with the samples prepared without any template.[24] By introducing TiO_2 species into WO_3 films, although coloration efficiency decreases slightly, the lifetime of WO_3–TiO_2 films can be five times longer than that of the pure WO_3 film.[25] Titanium-doping effects in electrochromic pulsed spray pyrolysis WO_3 thin films were examined, and the coloration efficiency was found to decrease with an increase in the Ti concentration.[26] The discharge corresponding to the electrochemical insertion of Li^+ shows a different behavior in the structural difference of WO_3–TiO_2 phases.[27] Spray-deposited TiO_2-doped WO_3 thin films varied from 13% to 38% in Ti content (mole ratio), and the coloration efficiency almost doubled in highly doped samples.[28]

Preparation method

In previous reports, electrochromic films were prepared by sol–gel method,[29] dip-coating,[30] hydrothermal method,[31] spin-coating,[32] sputtering,[33] chemical vapour deposition,[34] and pulsed-electrodeposition.[35] To the best of our knowledge, pulsed laser deposition method has not been reported for

State Key Laboratory of Inorganic Synthesis and Preparative Chemistry, College of Chemistry, Jilin University, Changchun 130012, P. R. China. E-mail: houcm@jlu.edu.cn; Fax: +86-431-85168624; Tel: +86-431-85168604

electrochromic film preparation, although it is widely used because of its homogeneity and good control of film quality in other film-related applications.[36]

In this paper, pure and TiO_2-doped WO_3 films were prepared *via* pulsed laser deposition method by controlling the thickness and surface morphology. Electrochromism properties were tested, and the films showed quick response to the applied voltage in dilute H_2SO_4 glycerol solution. The colored state of the films showed different blue color depending on the doping level of TiO_2 from dark blue (pure and 2% TiO_2-doped WO_3 film) to gem blue (5% and 10% TiO_2-doped WO_3 film). The crystal structure of the as-prepared films changed from triclinic WO_3 phase to cubic phase H_xWO_3 during coloration in all the samples.

2. Experimental

Chemicals and target preparation

Chemicals. Analytical grade H_2SO_4, glycerol (CH_2OH–$CHOH$–CH_2OH), TiO_2 and WO_3 powder were purchased from Sinopharm Chemical Reagent Co., Ltd. ITO glass and molybdenum plate (used as working and counter electrode, respectively) were purchased from Hefei Kejing Materials Technology Co., Ltd. All the chemicals were used without further purification.

Target preparation. For target preparation, stoichiometric amounts of TiO_2 and WO_3 were mixed in an agate mortar by repeated grinding for 3 h, and then the mixed powders were poured into a stainless steel mould with an inner diameter of 1 inch. The target was prepared by repeated calcination and grinding of WO_3 and TiO_2 powders for at least 3 times. The as-pressed targets of pure and TiO_2 doped WO_3 were calcined at 900 °C for 5 h, followed by 1000 °C for 1 h with the temperature increasing and decreasing rate of 5 °C min^{-1} After the targets were cooled to room temperature, they were immediately transferred into the chamber of pulsed laser deposition system.

Film preparation by PLD. Pulsed laser deposition of the electrochromic films was performed by using a COMPexPro205 excimer laser (Coherent cooperation, United States) and Pioneer 180 deposition chamber (Neocera cooperation, United States). Strips of ITO glass (1 cm × 1 cm) were cut and cleaned in four steps of 10 min each in ultrasonicated acetone, ethanol, 1 : 1 solution of H_2O_2 and ammonia, and ultrapure water. The cleaned ITO substrates were dried in N_2 flow and clayed to a round plate by a silver glue and baked for 10 min for fastening the ITO glass. The distance between the target and substrates was 75 mm. Before the film growth process, the ITO glass was heated at a rate of 25 °C min^{-1} to 500 °C for 0.5 h. The chamber pressure was maintained at 19.551 Pa when the laser ablation process was carried out on the targets. 10 000 shots of each film were performed on different targets, followed by further calcination in the chamber under an oxygen pressure of 53.2 kPa at 500 °C for 2 h.

Characterization

AFM. Atomic force microscopy (AFM) images were obtained using a SPA-400 (Seiko, Japan) multiple function unit together with SPI-3800N control station in tapping mode in air. The acquired AFM topology graphs were analyzed for roughness with SPA400 SPIWIN software from Seiko Ltd., Japan.

SEM. Scanning electron microscopy (SEM) images were obtained using a Helios NanoLab 600i Dual Beam System, FEI Company, America.

XRD. Powder X-ray diffraction (XRD) data were collected on a Rigaku D/Max 2500 V/PC X-ray diffractometer with Cu Kα radiation ($\lambda = 1.54718$ Å) with 50 kV and 200 mA at a scan speed of 1° per minute at room temperature. The step scanning angle was in the range of $20° \leq 2\theta \leq 70°$ with an increment of 0.02°.

XPS. X-ray photoelectron spectroscopy (XPS) was performed by using an ESCALAB 250 spectrometer with a mono X-ray source Al Kα excitation (1486.6 eV). Binding energy calibration was based on C 1s at 284.6 eV.

UV-Vis spectrum. UV-Vis absorption spectra were obtained using a Shimadzu 3100 UV-Vis spectrophotometer. For comparison, ITO glass was measured under the same conditions.

Electrochromic measurement

Electrochromic measurement was performed at room temperature with an applied voltage of 1 V for several minutes by a Keithley-2400 Source Meter (Keithley Instrument Inc.). H_2SO_4 : glycerol = 1 : 3 (volume ratio) solution was prepared as the electrolyte solution during the electrochromism processes. Electrode distance of the working electrode (electrochromic films) and the counter electrode (molybdenum plate: 3 × 6 cm^2) was 20 cm, and the applied voltage was 1 V. The electrical current and resistance between the counter electrode and film were monitored simultaneously by a Keithley source meter.

3. Results and discussion

3.1 Morphology analysis

AFM. The surface morphology of the as-prepared films was analyzed with atomic force microscopy (AFM) in 1 μm × 1 μm dimensions (Fig. 1). The films had uniform grain sizes on the surface within 40–60 nm for all the films, which is considerably more uniform than spin coatings. Root mean square roughness values were obtained by analyzing the topology of the as-prepared films in SPI 4000 (Version 4.08D) software of Seiko Instruments Inc. The surface roughness of films were 6.749, 6.036, 5.224 and 6.922 nm for pure WO_3, 2% TiO_2, 5% and 10% doped WO_3, respectively. The as-prepared films were uniform in thickness and had strong attachment to the ITO glass surfaces, which made them suitable for further applications.

Top-view SEM graphs. According to the SEM graphs (Fig. 2), all the films showed poly-crystalline surfaces with different nanostructure topologies. When the composition of TiO_2 was increased, small nanocrystalline grains gradually combined with each other and crevices occurred in the pure WO_3 film (Fig. 2(a)), 2% (Fig. 2(b)) and 10% (Fig. 2(c)) TiO_2-doped WO_3. The resulting crevice may induce more effective contact between the electrochromism layer and the electrolyte solutions. At the micrometer scale, however, they show a uniform and smooth morphology over the entire surface; thus,

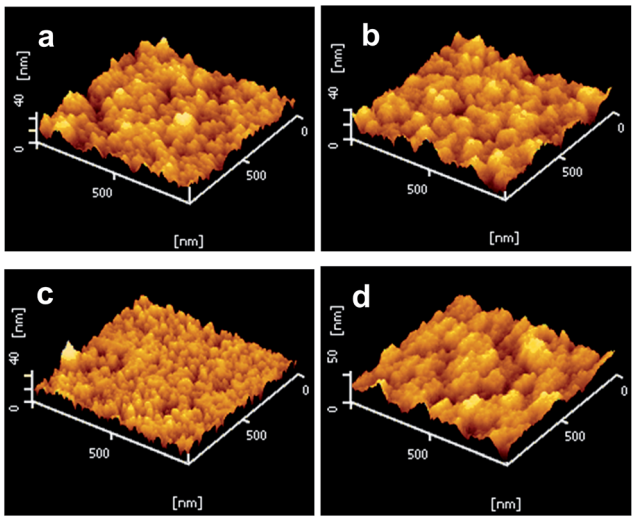

Fig. 1 Atomic force microscopy surface topology graphs of electrochromic films of (a) pure WO_3, (b) 2%, (c) 5% and (d) 10% TiO_2-doped WO_3. All the AFM graphs are shown with a tilt angle of 37°.

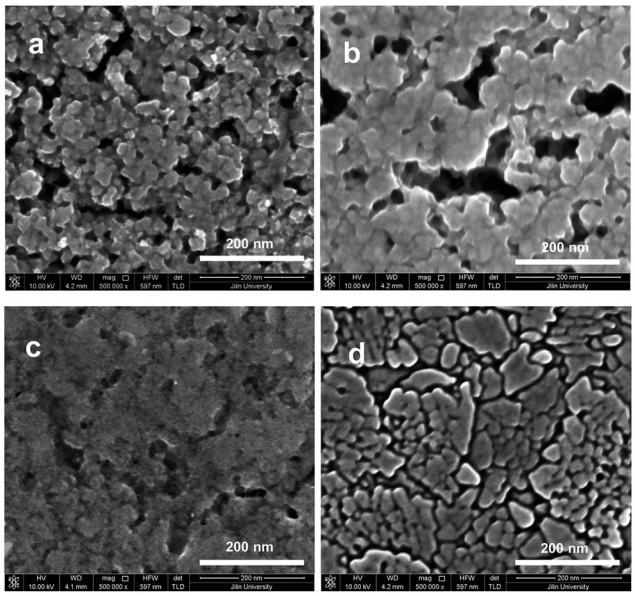

Fig. 2 Scanning electron microscopy graphs of as-prepared electrochromic films of (a) pure WO_3, (b) 2%, (c) 5% and (d) 10% TiO_2-doped WO_3.

transparency would not be affected significantly by growing the oxide layer.

Composition analysis

The film composition was analyzed by surface energy dispersive X-ray spectrum (EDX) equipped within the scanning electron microscope. W, Ti, O and In elements were identified according to their characterized X-ray energies excited by primary electrons emitted from SEM source. The intensity and peak area of the K-shell of Ti elements at *ca.* 4.5 keV increases along with the starting mixture composition in each target. Percentage of Ti/(Ti + W) content was calculated based on the peak area of the K-shell of Ti and the M-shell of W elements. The L-shell of In signal is from the substrate of ITO glass. In Fig. 3(a), (b) and (d), a stronger signal was detected than in Fig. 3(c), which may be attributed to fewer cracks in the 5% TiO_2-doped film, as shown in Fig. 2. With regard to other films, the surface film shielding effect was much weaker due to different percentages of cracks.

Cross-sectional view of the as-prepared films

The cross-sections of the as-prepared films were measured in SEM, as shown in Fig. 4, which indicates that all the films grew well on the substrate. Because of the difference in the atomic number of W in films and In, Sn in ITO, the contrast between ITO and film layers is apparent. As can be seen from each film, the electrochromism layer is not as compact as ITO, which may induce more interaction positions between the electrolyte solution and the colored material layers. The thicknesses for undoped and 2%, 5%, 10% TiO_2-doped WO_3 films were 238.5, 219.99, 240.83 and 224.55 nm, respectively. The thickness value was estimated as the average number counted for 10 different positions in each film. The close contact between ITO and tungsten oxides makes a firm connection between the two layers.

3.2 Electrochromic process analysis

Colored state. Current and resistance, as a function of the coloration time of pure and TiO_2-doped WO_3 films, are depicted in Fig. 5. The applied voltage was 1 V and there was a sharp response within 5 s, corresponding to ionic transportation process in high concentration. With an increase in the coloration time, the resistance value of each film became higher. This is because the concentration of conducted ions in solutions became lower due to the polarization effect in electrode (cathode) and films (anode). The highest value of polarization resistance of the films in the electrolyte solution was observed

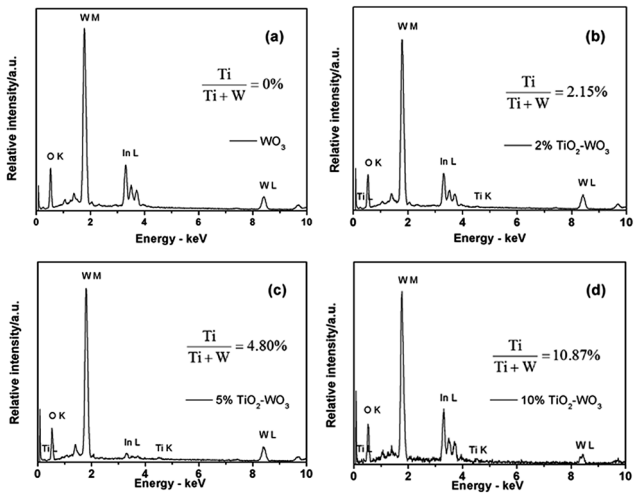

Fig. 3 Energy dispersive X-ray spectrum (EDX) of the as-prepared thin films: (a) pure WO_3, (b) 2% TiO_2, (c) 5% TiO_2 and (d) 10% TiO_2-doped WO_3 films.

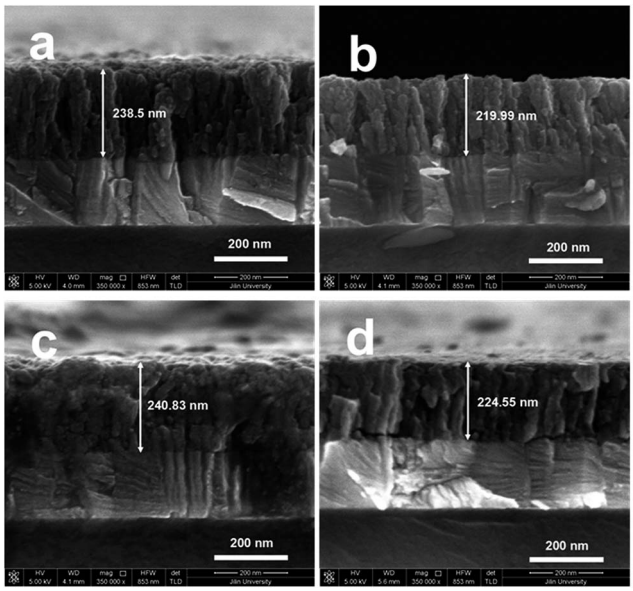

Fig. 4 Cross-section of the as-prepared films with (a) pure WO_3, (b) 2% TiO_2-doped WO_3, (c) 5% TiO_2-doped WO_3, and (d) 10% TiO_2-doped WO_3. Marked double arrow lines are given according to the scale bars.

in 2% TiO_2-doped WO_3. The increased resistance possibly resulted from the different polarization effect of the surface micro-structure. Detailed explanations require further atomic scale structural investigation based on highly advanced characterization techniques.

Bleached state. Fig. 6 illustrates the bleaching process of current and resistance, depending on applied voltage time. Quick response in all the films by an applied voltage of 1 V between the film and the counter electrode was within 5 s, which is because of the charge migration process induced by ion transport between the films and the counter electrode in the media solution. Resistance of all the films increased with elongated bleaching time, wherein 10% TiO_2-doped WO_3 and pure WO_3 films showed a greater resistance response after a 50 s bleaching state.

The current/resistance responses of the as-prepared films were in similar circumstance during coloration and bleaching processes at each TiO_2-doped level, which indicates a structural effect that influences the native coloration reaction rate and ion injection process in the crystal lattices.

3.3 Structural analysis

Pure WO_3 and colored WO_3 XRD analysis. Fig. 7 gives the diffraction spectrum of pure WO_3 film, which shows a triclinic

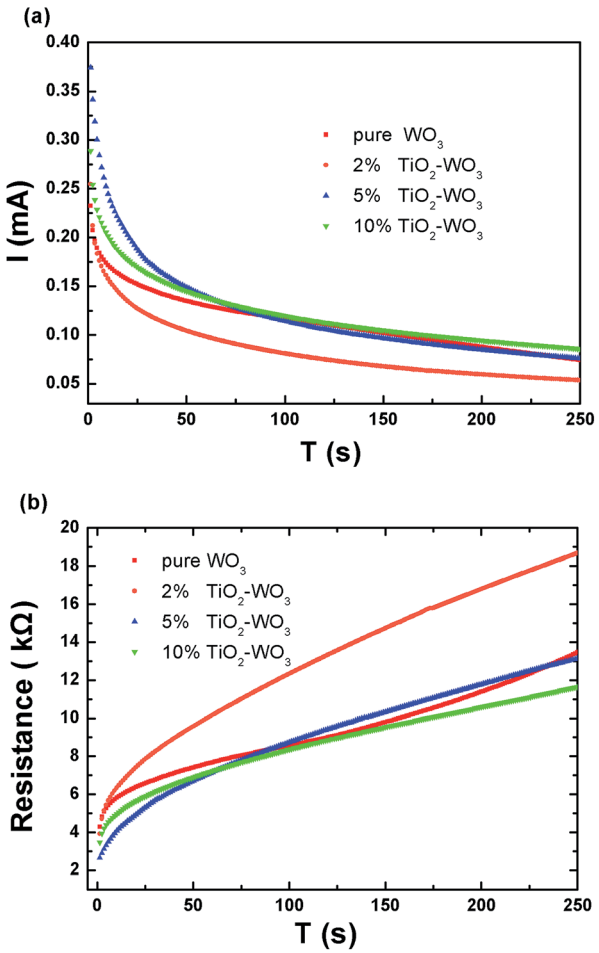

Fig. 5 Current (a) and resistance (b) changes dependent on increasing time of coloration of the as-prepared electrochromic films.

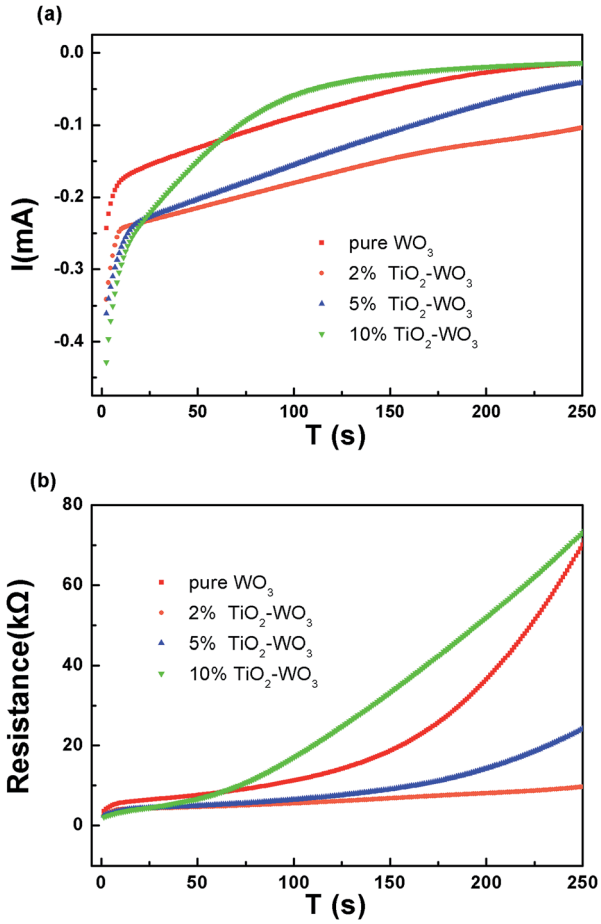

Fig. 6 Current (a) and resistance (b) changes dependent on increasing time of bleaching of the as-prepared electrochromic films.

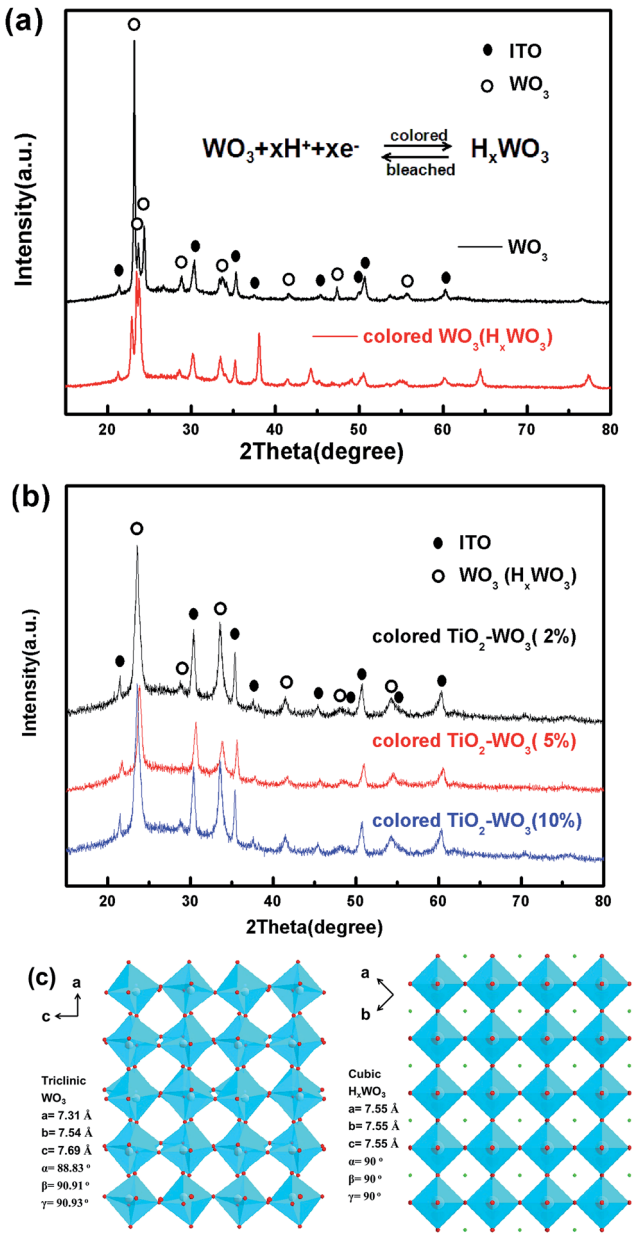

Fig. 7 XRD analysis of electrochromism processes of pure and TiO_2-doped WO_3 film: (a) structural changes in pure WO_3 film before and after coloration process; (b) XRD pattern of the colored films of 2%, 5% and 10% TiO_2-doped WO_3. Peak positions of WO_3 and ITO are marked with open and closed black circles, respectively. (c) Structure schemes of WO_3 and H_xWO_3 crystal cell evolution when H^+ is inserted into the lattice of pure tungsten trioxide. White balls: W; red balls: O and green balls: H.

polycrystalline structure. All the peaks in this pattern could be indexed as pure triclinic tungsten trioxide with the calculated lattice constants of $a = 7.31$, $b = 7.54$, $c = 7.69$ Å and $\alpha = 88.83°$, $\beta = 90.91°$, $\gamma = 90.93°$ (JCPDS no. 20-1323). Distorted octahedrals of WO_6 were corner-connected to each other, forming a relatively hollow space at the center enclosed by eight WO_6 octahedrals (Fig. 7(c)).

Compared with bleached WO_3 films, in colored WO_3, the crystal structure changed from a triclinic phase to a cubic phase of tetrahedral hydrogen bronze. This is because during the colored process, H^+ was inserted into the WO_3 lattice by the driving force generated from the electric field between the counter electrode and the film, which led to the formation of H_xWO_3. The related chemical reaction equation is shown in the inset of Fig. 7(a). The crystal structure of H_xWO_3 is cubic phase due to the insertion of H^+ into WO_3 lattice at the center of WO_6 octahedral. Unit cell parameters of a, b, and c did not change significantly due to the small radius of H^+ (Fig. 7(c)).

Colored TiO_2-doped WO_3 film structure analysis. The XRD patterns of colored TiO_2-doped WO_3 films are shown in Fig. 7. All the as-prepared films adopted the same crystal structure as colored pure WO_3 film (colored WO_3 peaks of XRD are marked with open circles). The films are well-crystallized, and on increasing the TiO_2 composition, the structure remains stable. No recognizable TiO_2 phase was seen in the XRD patterns of all the films, which implies that the Ti species possibly existed in the films either as interstitial or as amorphous composite separated by assembled WO_3 polycrystalline grains.

3.4 XPS analysis

Binding energy changes induced by H^+ insertion into the crystal lattice were characterized by X-ray photoemission spectroscopy. As H^+ ions and electrons flow into the lattice of WO_3 and TiO_2-doped WO_3 films, some W^{6+} ions are reduced to W^{5+} and even W^{4+}, and polarize the surrounding lattice to form small structure and valence distortions. According to XPS data, discrete valence states of W in colored and bleached WO_3 films were identified. The colored state of WO_3 film incorporated H^+ into the lattice, which formed a bronze structure of H_xWO_3. H^+ in lattice reduced the valence state of W, which made W a mixed state of +6, +5 and +4 (Fig. 8). The binding energy peak positions of $W_{4f_{5/2}}{}^{5+}$ and $W_{4f_{7/2}}{}^{6+}$ were 38.03 eV and 35.85 eV, respectively. The effect of coloration is reflected in the extremely high asymmetry of the peak profile, which suggests a high concentration of W^{5+} and W^{4+} states in the film formed at the cost of the W^{6+} states. The appearance of a third component at 33.5 and 35.7 eV for $W_{4f_{7/2}}$ and $W_{4f_{5/2}}$, respectively, confirms the presence of W^{4+} states in the colored film in addition to the W^{5+} and W^{6+} states. On comparing the colored state to the bleached state of pure WO_3 film, the relative composition of W^{6+}, W^{5+} and W^{4+} were 69.72%, 17.04% and 13.24%. There is a linear correlation between the increase in $W_{4f_{5/2}}{}^{5+}$ and the insertion coefficient x (H_xWO_3) for $x < 0.25$.[37] W^{5+} state is assumed to be the color center in WO_3, and a large W^{5+} content (17.04%) in this film (Fig. 8(b)) as compared with a low W^{5+} concentration in its uncolored or virgin state is responsible for the dark blue color (Fig. 9) acquired by the film upon H^+ insertion.

3.5 Ultraviolet-visible spectroscopy

To determine the visible absorption regions of the spectrum, ultraviolet-visible spectroscopy was characterized in colored and bleached films. Compared with bleached pure WO_3 films, the colored ones show enhanced absorption in the entire range of the spectrum from 200 to 1000 nm (Fig. 9(a)). A broad peak appears between 300 and 600 nm, especially at 400–500 nm,

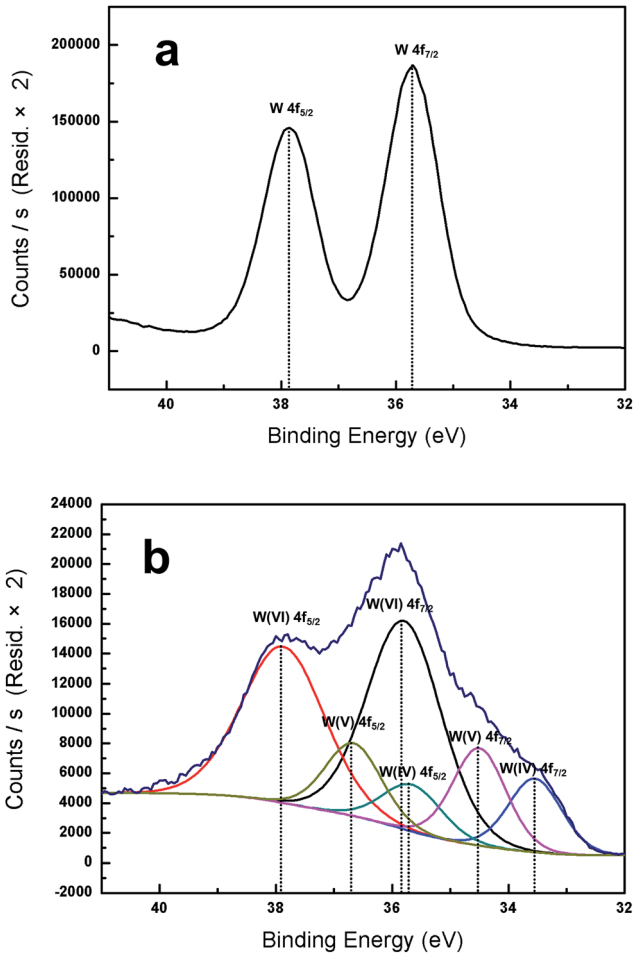

Fig. 8 XPS analysis of the as-prepared electrochromic pure WO_3: (a) bleached state; (b) colored state. All the peak positions are marked by vertical dotted lines.

which is the primary blue spectrum position. With TiO_2-doping, the strong absorption peaks shift left from *ca.* 250–370 nm in 5% and 10% doped films. Moreover, there is a strong broad peak at 600–700 nm absorption in these samples, which may account for the occurrence of gem-blue color in the 5% and 10% doped films.

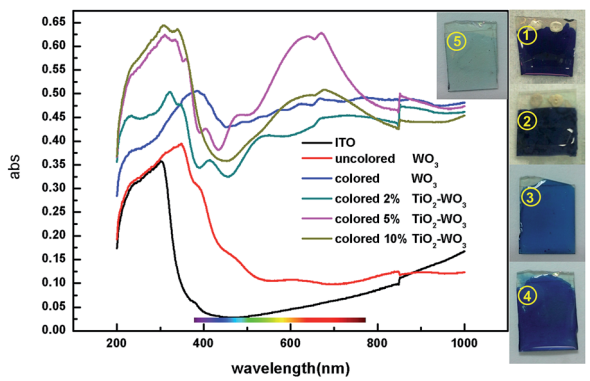

Fig. 9 Ultraviolet-visible spectroscopy of the electrochromic films: absorption of ultraviolet-visible spectrum of TiO_2-doped WO_3 films, ITO was tested for the comparison of the substrate. The right part shows digital graphs: colored ① pure WO_3, ② 2%, ③ 5% and ④ 10% TiO_2-doped WO_3 films, ⑤ bleached pure WO_3 film.

The absorption peak of ITO glass was at *ca.* 300 nm and no other peaks could be recognized in the entire visible light wavelength scale (390–770 nm). Thus, the ITO glass is transparent at room temperature. The as-prepared pure WO_3 film shows an absorption peak at 370 nm, and the whole absorption curve is considerably higher in the entire scale of visible light wavelength, which indicates a weaker transparent degree. A peak shift appears toward the red light wavelength in the colored pure WO_3 film, and a wide absorption peak is mainly at 400–450 nm. This peak should be red-yellow according to the dominant wavelength and complementary wavelength in color theory. The entire curve of the pure colored WO_3 film shows high absorption, and the peak is not so evident compared to the long wavelength absorption (the absorption value keeps increasing after about 470 nm), which makes the film a dark blue in color. For 2% TiO_2-doped WO_3 film, the peak appears at 310–320 nm, which is 390 nm of pure WO_3; by TiO_2-doping, the peak shifts to purple color direction. However, the peak is beyond the visible light wavelength scale and shows no contribution to color change. At a region of more than 500 nm, a much stronger absorption appears, but no peaks can be recognized. A valley appears at 410 and 460 nm, which indicates the weak absorption of blue-purple light, and the color finally turns dark blue. For the 5% TiO_2-doped WO_3 film, the absorption intensity increased at the full scale of the wavelength, which implies that TiO_2 absorbed more light than WO_3. The peak at 300 nm was wide, indicating that the Ti species absorbed ultraviolet wavelength light, and the results have been accepted in many TiO_2-related catalysis applications. The absorption was weak at blue-violet wavelength and increased after 500 nm with a peak at 620–700 nm, which belongs to the red-yellow wavelength scale. According to the complementary color rule, it will appear as blue when absorption is red and yellow. Thus, the 5% TiO_2-doped WO_3 shows the gem blue color. By further increasing TiO_2-doping level to 10%, although the shapes of the absorption curves were the same compared with the 5% doped film, the peak weakened at the red-yellow wavelength scale, accounting for the relatively deeper gem blue color. Thus, by accommodating the TiO_2-doped level to WO_3 films, the color and absorption of visible light was altered from dark blue to gem blue.

4. Conclusions

In conclusion, pure and TiO_2-doped WO_3 films were prepared by pulsed laser deposition using a target of mixed ceramics. The films have a narrow distribution of particle size and can be produced on a large scale by a single process. An electrochromic process was performed and the current/resistance changes throughout the colorizing/bleaching experiment were monitored. Structural changes from triclinic phase WO_3 to the tungsten–bronze phase of H_xWO_3 were incurred by coloration. In the colored state, the valence of W showed mixed valence of +6, +5 and +4. The films can be bleached with quick response

and cycled for at least 1000 times. Ultraviolet-visible spectroscopy demonstrates that the colored films show strong absorption at 380–450 nm, which makes the film blue in color. This study is valuable for applications in smart windows and colored displays.

Acknowledgements

This work was supported by the National Natural Science Foundation of China (Grants 21131002 and 21201075) and the Specialized Research Fund for the Doctoral Program of Higher Education (SRFDP Grant 20110061130005).

Notes and references

1 R. J. Mortimer, *Annu. Rev. Mater. Res.*, 2011, **41**, 241–268.
2 C. G. Granqvist, A. Azens, P. Heszler, L. B. Kish and L. österlund, *Sol. Energy Mater. Sol. Cells*, 2007, **91**, 355–365.
3 D. R. Rosseinsky and R. J. Mortimer, *Adv. Mater.*, 2001, **13**(11), 783–793.
4 P. Audebert and F. Miomandre, *Chem. Sci.*, 2013, **4**, 575–584.
5 T. Yamase, *Chem. Rev.*, 1998, **98**, 307–325.
6 G. A. Niklasson and C. G. Granqvist, *J. Mater. Chem.*, 2007, **17**, 127–156.
7 P. Andersson, R. Forchheimer, P. Tehrani and M. Berggren, *Adv. Funct. Mater.*, 2007, **17**, 3074–3082.
8 P. M. Beaujuge and J. R. Reynolds, *Chem. Rev.*, 2010, **110**, 268–320.
9 V. K. Thakur, G. Q. Ding, J. Ma, P. S. Lee and X. H. Lu, *Adv. Mater.*, 2012, **24**, 4071–4096.
10 P. Andersson, D. Nilsson, P. O. Svensson, M. X. Chen, A. Malmstrom, T. Remonen, T. Kugler and M. Berggren, *Adv. Mater.*, 2002, **14**, 1460–1464.
11 P. Tehrani, L. O. Hennerdal, A. L. Dyer, J. R. Reynolds and M. Berggren, *J. Mater. Chem.*, 2009, **19**, 1799–1802.
12 M. Deepa, A. K. Srivastava, S. Lauterbach, Govind, S. M. Shivaprasad and K. N. Sood, *Acta Mater.*, 2007, **55**, 6095–6107.
13 M. Z. Najdoski and T. Todorovski, *Mater. Chem. Phys.*, 2007, **104**, 483–487.
14 A. Ghicov, S. P. Albu, J. M. Macak and P. Schmuki, *Small*, 2008, **4**(8), 1063–1066.
15 S.-Y. Lin, Y.-C. Chen, C.-M. Wang and C.-C. Liu, *J. Solid State Electrochem.*, 2008, **12**, 1481–1486.
16 M. Maček, B. Orel and U. Opara Krašovec, *J. Electrochem. Soc.*, 1997, **144**(9), 3002–3010.
17 J. N. Yao, Y. A. Yang and B. H. Loo, *J. Phys. Chem. B*, 1998, **102**, 1856–1860.
18 F. Lin, D. Nordlund, T.-C. Weng, D. Sokaras, K. M. Jones, R. B. Reed, D. T. Gillaspie, D. G. J. Weir, R. G. Moore, A. C. Dillon, R. M. Richards and C. Engtrakul, *ACS Appl. Mater. Interfaces*, 2013, **5**, 3643–3649.
19 A. Chemseddine, M. Henry and J. Livage, *Rev. Chim. Miner.*, 1984, **21**, 487.
20 J. Livage and G. Guzman, *Solid State Ionics*, 1996, **84**, 205–211.
21 H. Wang, M. Zhang, S. Yang, L. Zhao and L. Ding, *Sol. Energy Mater. Sol. Cells*, 1996, **43**, 345–352.
22 Z. Wang and X. Hu, *Electrochim. Acta*, 2001, **46**, 1951–1956.
23 (*a*) T. Todorovski and M. Najdoski, *Mater. Res. Bull.*, 2007, **42**, 2025–2031; (*b*) M. Z. Najdoski and T. Todorovski, *Mater. Chem. Phys.*, 2007, **104**, 483–487.
24 C.-S. Hsu, C.-K. Lin, C.-C. Chan, C.-C. Chang and C.-Y. Tsay, *Thin Solid Films*, 2006, **494**, 228–233.
25 (*a*) C. G. Granqvist, *Handbook of Inorganic Electrochromic Materials*, Elsevier, Amsterdam, 1995; (*b*) A. Karuppasamy and A. Subrahmanyam, *Thin Solid Films*, 2007, **516**, 175–178.
26 S. R. Bathe and P. S. Patil, *Solid State Ionics*, 2008, **179**, 314–323.
27 B. Yebka, B. Pecquenard, C. Julien and J. Livage, *Solid State Ionics*, 1997, **104**, 169–175.
28 P. S. Patil, S. H. Mujawar, A. I. Inamdar and S. B. Sadale, *Appl. Surf. Sci.*, 2005, **250**, 117–123.
29 M. A. Aegerter, C. O. Avellaneda, A. Pawlicka and M. Atik, *J. Sol-Gel Sci. Technol.*, 1997, **8**, 689–696.
30 H. Wang, M. Zhang, S. Yang, L. Zhao and L. Ding, *Sol. Energy Mater. Sol. Cells*, 1996, **43**, 345–352.
31 J.-Z. Chen, W.-Y. Ko, Y.-C. Yen, P.-H. Chen and K.-J. Lin, *ACS Nano*, 2012, **6**(8), 6633–6639.
32 K. Nagase, S. Izaki, Y. Shimizu, N. Miura and N. Yamazoe, *J. Mater. Chem.*, 1994, **4**(10), 1581–1584.
33 V. Teixeira, H. N. Cui, L. J. Meng, E. Fortunato and R. Martins, *Thin Solid Films*, 2002, **420**, 70–75.
34 K. A. Gesheva and T. Ivanova, *Chem. Vap. Deposition*, 2006, **12**, 231–238.
35 S. H. Baeck, T. Jaramillo, G. D. Stucky and E. W. McFarland, *Nano Lett.*, 2002, **2**(8), 831–834.
36 R. Eason, *Pulsed Laser Deposition of Thin Films: Applications-Led Growth of Functional Materials*, John Wiley & Sons, Inc., 2006, pp. 3–28, ISBN-10: 0-471-44709-9.
37 C. R. Ottermann, A. Temmink and K. Bange, *Thin Solid Films*, 1990, **193**, 409.

